J Neurophysiol 94: 1509–1518, 2005.
First published April 27, 2005; doi:10.1152/jn.00957.2004.

Slow and Fast Inhibition and an H-Current Interact to Create a Theta Rhythm in a Model of CA1 Interneuron Network

Horacio G. Rotstein,[1] Dmitri D. Pervouchine,[1] Corey D. Acker,[2] Martin J. Gillies,[3] John A. White,[2] Eberhardt H. Buhl,✠ Miles A. Whittington,[3] and Nancy Kopell[1]

[1]*Department of Mathematics and Statistics and* [2]*Department of Biomedical Engineering and Center for Biodynamics, Boston University, Boston, Massachusetts; and* [3]*School of Biomedical Sciences, University of Leeds, Leeds, United Kingdom*

Submitted 14 September 2004; accepted in final form 27 March 2005

Rotstein, Horacio G., Dmitri D. Pervouchine, Corey D. Acker, Martin J. Gillies, John A. White, Eberhardt H. Buhl, Miles A. Whittington, and Nancy Kopell. Slow and fast inhibition and an h-current interact to create a theta rhythm in a model of CA1 interneuron network. *J Neurophysiol* 94: 1509–1518, 2005. First published April 27, 2005; doi:10.1152/jn.00957.2004. The oriens-lacunosum moleculare (O-LM) subtype of interneuron is a key component in the formation of the theta rhythm (8–12 Hz) in the hippocampus. It is known that the CA1 region of the hippocampus can produce theta rhythms in vitro with all ionotropic excitation blocked, but the mechanisms by which this rhythmicity happens were previously unknown. Here we present a model suggesting that individual O-LM cells, by themselves, are capable of producing a single-cell theta-frequency firing, but coupled O-LM cells are not capable of producing a coherent population theta. By including in the model fast-spiking (FS) interneurons, which give rise to IPSPs that decay faster than those of the O-LM cells, coherent theta rhythms are produced. The inhibition to O-LM cells from the FS cells synchronizes the O-LM cells, but only when the FS cells themselves fire at a theta frequency. Reciprocal connections from the O-LM cells to the FS cells serve to parse the FS cell firing into theta bursts, which can then synchronize the O-LM cells. A component of the model O-LM cell critical to the synchronization mechanism is the hyperpolarization-activated h-current. The model can robustly reproduce relative phases of theta frequency activity in O-LM and FS cells.

INTRODUCTION

Field potential oscillations at theta frequencies (8–12 Hz) in the hippocampal formation have been correlated with various brain functions and behavioral states, including representation of visuospatial information (Kahana et al. 1999; O'Keefe and Nadel 1978; O'Keefe and Recce 1993; Skaggs et al. 1996), rapid eye movement (REM) sleep (Jouvet 1969), active exploration (Vanderwolf 1969), and memory formation and retrieval (Buzsáki 1989; Larson and Lynch 1986; Lisman and Idiart 1995; Raghavachari et al. 2001). The theta rhythm is most regular in frequency and largest in amplitude in the stratum lacunosum-moleculare of the hippocampal CA1 region (Buzsáki 2002, and references therein).

There are at least two forms of theta, both dependent on the medial septum in vivo: an atropine-sensitive form (presumably requiring a cholinergic input from the septum) and an atropine-resistant form, dependent on the entorhinal cortex and probably requiring *N*-methyl-D-aspartate (NMDA) receptors (Buzsáki et al. 1983). Although in vivo lesions of major input regions for the hippocampus and entorhinal cortex have profound effects on hippocampal/entorhinal theta (Buzsáki et al. 1983; Lee et al. 1994), this does not imply that these regions are the only source of the theta rhythm. In addition to imposition of theta rhythms on the hippocampus by the septum and the entorhinal cortex, there are a variety of dynamical mechanisms intrinsic to the hippocampal formation that allow networks to create or resonate to rhythms in that frequency range, possibly with anatomically separate generators of similar rhythms (Csisvari et al. 2003; Kocsis et al. 1999).

The entorhinal cortex (EC), CA1, and CA3 all have cells that are capable of producing oscillations in the theta-frequency regime. The EC has excitatory spiny stellate cells, which are also able to generate single-cell theta oscillations (Alonso and Llinás 1989). CA1 and CA3 have a variety of inhibitory cell types believed to be able to produce single-cell oscillations (Banks et al. 2000; Chapman and Lacaille 1999a,b; Gillies et al. 2002; White et al. 2000b). Under the appropriate pharmacological circumstances, hippocampal brain slices generate synchronized activity at theta frequencies (Fellous and Sejnowski 2000; Gillies et al. 2002; Konopacki et al. 1987; Williams and Kauer 1997).

Of particular interest for this paper is the work of Gillies et al. (2002) concerning an atropine-resistant theta produced in an in vitro model (CA1). In their experiments they used metabotropic receptor activation combined with α-amino-3-hydroxy-5-methyl-4-isoxazolepropionic acid (AMPA) receptors blockade, which suppresses gamma oscillations that would otherwise occur (Gillies et al. 2002). This work demonstrated a theta rhythm generated by the internal circuitry within area CA1 alone. The profile of the theta rhythms seen bore a number of similarities to theta rhythms seen in vivo. *1*) A sharp phase reversal in midstratum radiatum (Buzsáki et al. 1986). *2*) Pyramidal cell spike timing with reference to the field theta rhythm and a distinct pattern of spike timings for fast spiking and oriens-lacunosum moleculare (O-LM) interneurons (Bragin et al. 1995; Fox et al. 1986; Harris et al. 2000). *3*) Dendritic electrogenesis in pyramidal cells (Kamondi et al. 1998). The study by Gillies et al. (2002) implicated O-LM cells as critical for the theta rhythm generated internally within area CA1. These cells have a strong intrinsic theta rhythm (Maccaferri and McBain 1996; Saraga et al. 2003) that leads to them generating theta-frequency outputs during field gamma

✠ Deceased 18 January, 2003.

Address for reprint requests and other correspondence: H. G. Rotstein, Department of Mathematics and Statistics and Center for Biodynamics, Boston University, Boston, MA 02215 (E-mail: horacio@math.bu.edu).

The costs of publication of this article were defrayed in part by the payment of page charges. The article must therefore be hereby marked "*advertisement*" in accordance with 18 U.S.C. Section 1734 solely to indicate this fact.

rhythms as well as in theta experimental models of theta rhythms (Gillies et al. 2002; T. Gloveli, T. Dugladze, H. G. Rotstein, R. D. Traub, H. Monyer, U. Heinemann, M. Whittington, and N. Kopell, unpublished data). The outputs from these cells, whose bodies are in stratum oriens, are projected as slow inhibitory postsynaptic potentials (IPSPs) onto the distal dendrites of pyramidal neurons (Whittington and Traub 2003). O-LM cells also have axonal projections to the lacunosum moleculare layer, and some axon collatorals in the stratum oriens (Hájos and Mody 1997); the latter provide an anatomical substrate for synaptic connections among O-LM cells.

The purpose of this paper is to examine the biophysical mechanism of production of the coherent theta oscillations in the in vitro CA1 preparation. Thus, we are concerned with both the intrinsic properties of the interneurons and the dynamical mechanisms that create coherence. In the data of Gillies et al. (2002) cells do not fire in absolute synchrony. Rather, there is a loose pattern of spikes of different kinds of interneurons (shown in Fig. 4*A,* to be discussed below), which we call "ragged synchronization."

We shall show that the mechanism we propose can account for details of this loose coherence. The results of the paper depend critically on the slow, hyperpolarization-activated mixed cation current I_h, known to be expressed in O-LM cells (Gillies et al. 2002; Saraga et al. 2003). This current is important because it changes the synchronization properties of the cells that express it (Acker et al. 2003; Crook et al. 1998; HG Rotstein, T Oppermann, JA White, and N Kopell, unpublished data): whereas models of cells with only simple spiking currents synchronize well with inhibition, but not excitation, the opposite is true when model cells express certain slow currents, including I_h (Acker et al. 2003; Crook et al. 1998; Rotstein et al., unpublished data). I_h is also important because it changes the response of the cell to inhibition: instead of delaying spikes, the inhibition can cause spikes to arrive faster. In the network of O-LM and fast-spiking interneurons we investigate, both effects of I_h play a large role.

METHODS

Experimental

Transverse hippocampal slices (450 μm) were prepared from adult Wistar rats, anesthetized with inhaled isoflurane, immediately followed by an intramuscular injection of ketamine ($\geq$100 mg kg^{-1}) and xylazine ($\geq$10 mg kg^{-1}) and transferred to a recording chamber. Here, they were maintained at 34°C at the interface between a continuous stream (1.2 ml/min) of artificial cerebrospinal fluid (ACSF) [composition in mM: NaCl (126), KCl (3), NaH_2PO_4 (1.25), $NaHCO_3$ (24), $MgSO_4$ (2), $CaCl_2$ (2), and glucose (10)], and warm, moist carbogen gas (95% O_2-5% CO_2). Slices were permitted to equilibrate for 45 min before any recordings commenced. Theta oscillations in area CA1 were induced by bath application of DHPG [(S)-3,5-dihydroxyphenylglycine] 60 μM and NBQX (2,3-dioxo-6-nitro-1,2,3,4-tetrehydrobenzo[f]quinoxaline-7-sulfonamide) 20 μM, both from Tocris (Bristol, UK). Extracellular recordings of theta activity were taken from stratum pyramidale using glass electrodes filled with ACSF (resistance 2–5 MΩ). Intracellular recordings from somata of pyramidal neurons and FS interneurons with cell bodies in stratum pyramidale were taken with glass electrodes filled with KCH_3SO_4 (resistance 70–130 MΩ).

Computational

The inhibitory network studied in this paper consists of N_O O-LM (O- cells) and N_I fast-spiking interneurons (I-cells). Each cell is modeled using the conductance-based Hodgkin–Huxley (HH) formalism. The dynamic equations are given in the Appendix. Both the O- and I-cells are described as one compartment having standard HH currents (transient *Na,* delayed rectifier *K,* and leak). For the O-cells, the modeling also incorporates a hyperpolarization activated current I_h with two components (slow and fast kinetics) and an additional current I_p, which is active during the interspike interval. The parameter range is chosen so that the h-current is necessary for an isolated O-cell to spike, as occurs in the experiments described in Gillies et al. (2002). The extra current I_p is modeled as the persistent sodium current in models of entorhinal spiny stellate cells (Acker et al. 2003). Spontaneous firing of O-neurons is known to occur at about 5–20 Hz. (Ali and Thomson 1998; Lacaille et al. 1987; Maccaferri and McBain 1996; Saraga et al. 2003). In most of the simulations presented here we follow Saraga et al. (2003) and choose the natural frequency of the O-cells (i.e., the frequency in the absence of synaptic inputs) to be about 12 Hz. However, these results are robust to changes in these natural frequencies. The cells are synaptically connected with IPSPs from O-cells lasting longer than those originating from I-cells. The decay times of O and I IPSPs (defined as the time it takes for the synaptic conductance to decrease to about 37% of its maximum value) are 20 and 10 ms, respectively (Hájos and Mody 1997; Traub et al. 1996). For the former there are no measurements of O–I IPSPs, and the 20-ms number we use for most of the simulations is taken from O to pyramidal cell connections; other values are investigated and discussed.

We consider all possible putative connectivity among the I-cells and O-cells. Some evidence for I–O and O–I connections are in the RESULTS section. O–O connections have not been found experimentally. As we show, the O–O connections, if present, do not help synchronization at theta frequencies for biologically plausible values of the parameters.

The network is globally connected (all-to-all connections) with heterogeneous synaptic connectivity. We create a spatial structure by ordering the cells as schematically shown in Fig. 4*C.* In our simulations the maximal synaptic conductances are larger the closer the cells are in the network (see Appendix). In Fig. 4*C* this heterogeneity is schematically represented by the thickness of the connections: the thicker the line, the stronger the connection; for O–O and I–I we show only the strongest connections. Note that for cells far enough apart, the synaptic connectivity may be close to zero. I-cells have autapses to account for some network inhibitory effects.

Large network simulations are performed using custom software implemented in Matlab and C using Matlab's application program interface (mex). This software is a flexible tool to rapidly simulate scalable networks of model neurons with easily variable network structure and connectivity. Numerical integration is performed in C using a standard adaptive step-size Runge–Kutta algorithm. Synapses are implemented using an efficient algorithm that affords tremendous improvements in simulation times for networks of single-compartment neurons (Lytton 1996). Small network simulations are performed using a Runge–Kutta method of order four (Burden and Faires 1980) and the XPP software (Ermentrout 2002).

RESULTS

A network of O-cells does not create a coherent theta rhythm

Figure 1 shows an example of the firing when a pair of O-cells (Fig. 1*A*) is coupled by inhibition. For each of two levels of coupling, antiphase patterns are formed (Fig. 1*B*). Note that the period of the network decreases with the increase

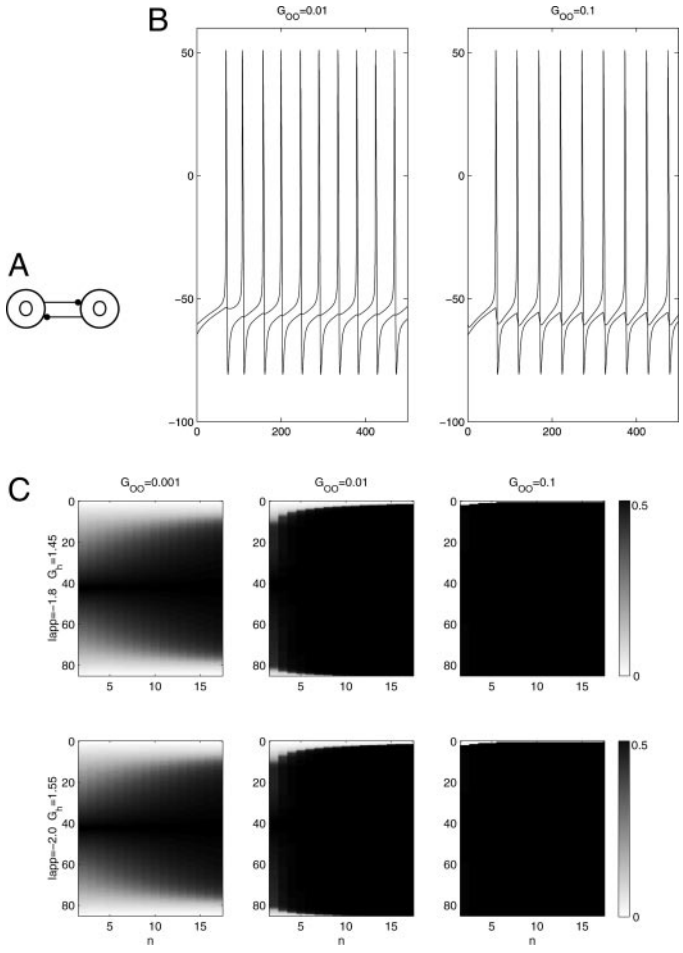

FIG. 1. Mutually coupled O-cells do not synchronize robustly. *A*: network of 2 O-cells. *B*: firing patterns of 2 synaptically coupled O-cells for different values of the maximal synaptic conductance (G_{OO}). Natural frequency of the O-cells is about 12 Hz. Values of the corresponding parameters are $G_h = 1.45$, $I_{app,O} = -1.8$. *C*: mutual inhibition leads to a very small domain of stability for the synchronous solution. We show the phase difference of spikes (color bar) in each cycle (abscissas) as a function of the initial phase difference (ordinates). Phase difference is defined as the difference in spiking times between the 2 O-cells normalized by the natural frequency of the uncoupled cells.

in coupling conductance. These results are robust for a large range of coupling strengths, natural frequencies of O-cells, and initial conditions. For initial conditions very close to synchrony, the cells do synchronize. However, that range of initial conditions is very small, and essentially disappears when the coupling conductance G_{OO} is set to at least 0.1 (Fig. 1*C*). As the number of cells in the O-network increases, the probability of finding all cells in the small basin of attraction of in-phase synchrony decreases; for cells initially in splay-phase two antiphase clusters are found (data not shown). Thus, with just O-LM cells in the network, synchrony is not robust. Although the network can robustly produce rhythms, when there is antiphase or clusters, the population frequency is higher than theta for physiological values of the parameters.

The nonsynchronization results persist when gap junctions are added, even with a gap junctional conductance large enough that the electrical coupling current during a spike is the same order of magnitude as the maximal inhibitory coupling current (data not shown).

Input from I-cells can sometimes synchronize O-cells

It is known that common inhibition can create synchrony (Chow et al. 1998; Gerstner et al. 1996; van Vreeswijk et al. 1994; Wang and Rinzel 1992; White et al. 1998). Figure 2*A* contains evidence that O-cells receive fast inhibition, presumably from the I-cells. In a network of I- and O-cells (Fig. 2*B*), the inhibition from the I-cells can indeed help to synchronize the O-cells. However, because of the hyperpolarization-activated current in the O-cells, the effect of inhibition on the O-cells is not straightforward: it depends on the frequency of the I-cell input, which interacts with the timescales of the I_h current. Some effects are shown below in Fig. 2; a more detailed mathematical treatment of these effects is in progress.

Figure 2*C* shows the network when a pair of O-cells starting in antiphase receives common inhibition at 8 Hz with the O-cells connected with $G_{OO} = 0.01$ (the results still hold with $G_{OO} = 0$). Note that the I-cell inhibition leads quickly to synchronization of the O-cells. This is true for input up to 13 Hz (with these parameters). The *bottom trace* of Fig. 2*C* shows the conductance of the h-current of each of the two O-cells. Note that the conductance increases quickly as the pulse of inhibition is received, and drops quickly right after the cell spikes.

The input from I-cells at higher frequencies (13–30 Hz) is fast enough to suppress some of the O-cell spikes. In this range of frequencies, the natural driving currents of the cell cannot withstand the inhibition. However, the hyperpolarization-activated current I_h comes into play. Each time there is a pulse of inhibition, this current builds up, until the cell fires (Kopell and LeMasson 1994); the O-cells may phase-lock to different cycles of the input from I-cells. This results in a pattern with a constant phase lag between the O-cells; the phase lag can be zero, if the cells start with very close initial conditions, but for more generic initial conditions the pattern is phase-locked rather than synchronous. Figure 2*D* shows this for an I-cell firing at about 28 Hz and imposing a coherent but not synchronous nearly 8-Hz pattern on the O-cells. The *right hand panels* of this figure shows the time course of I_h in two O-cells. At still higher input frequencies ($\gtrsim$28 Hz), the buildup of I_h may take many more cycles, and if the input frequency is sufficiently high, the O-cells may be completely suppressed (data not shown).

To summarize, at input frequencies starting from not much above that in the uncoupled O-cell, the inhibitory input may create synchrony of the O-cells, but not in a way robust to changes in input frequency or initial conditions. This is important because the frequency of the I-cell may go up to 70 Hz (Buzsáki and Chrobak 1995).

Feedback from O- to I-cells creates a more robust theta rhythm

Evidence for slow IPSPs onto I-cells is given in Fig. 3*A*. Although the O-cells produce such slow IPSPs (Gillies et al. 2002) it has not yet been experimentally shown that the IPSPs in Fig. 3*A* come from the O-cells. We hypothesize that they do.

The effects of the O $\rightarrow$ I feedback (Fig. 3*B*) depend on the strength of the feedback and the frequency. We focus on the parameter range in which the O $\rightarrow$ I coupling is not strong enough to suppress the spikes of the I-cells. If the I-cell firing

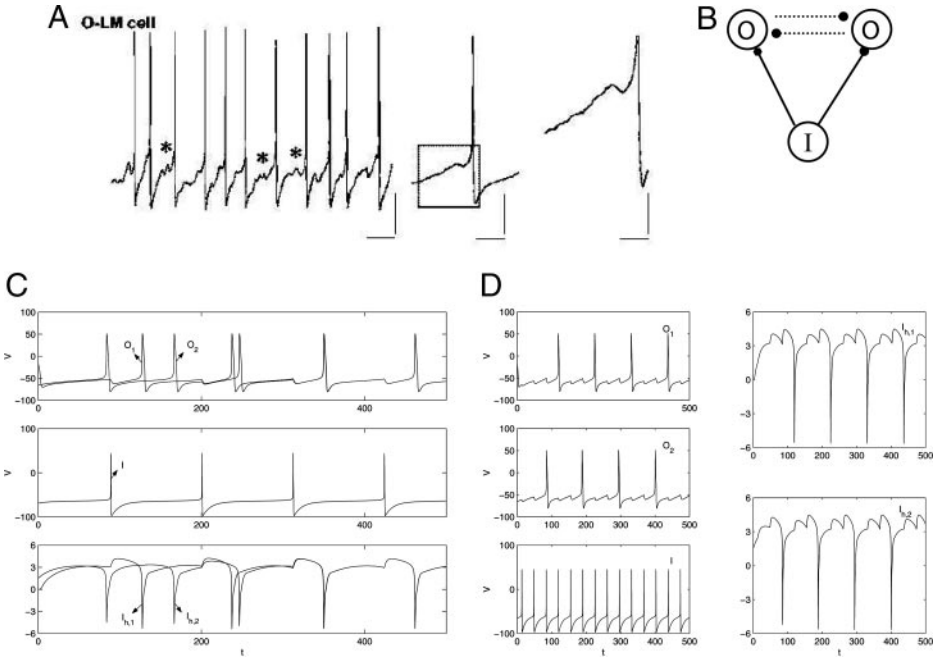

FIG. 2. Common fast-spiking (FS) inhibition to O-cells can cause synchronization. *A*: in vitro evidence for FS inhibition of the oriens-lacunosum moleculare (O-LM) cell. O-cells invariably fired one action potential per period. Spikes were preceded by trains of inhibitory postsynaptic potentials (IPSPs) (asterisks). *Average traces* ($n = 10$ periods averaged with respect to the O-cell spike) showed an IPSP occurring immediately before spike generation. Scale bars: spike train 10 mV, 100 ms; average 10 mV, 25 ms; expanded average 2 mV, 10 ms. *B*: FS cell gives common inhibition to 2 O-cells. *C*: I input at about 8 Hz to a network of 2 O-cells, $I_{app,I} = 0.154$, $G_{OO} = 0.01$, $G_{IO} = 0.2$, $G_{OI} = 0$, $G_h = 1.45$, $I_{app,O} = -1.8$. Natural frequency of each O-cell is about 12 Hz. Frequency of each O-cell in the O–O network (in the absence of I inputs) is about 10.5 Hz. *D*: input from an I-cell firing at about 28 Hz creates a coherent but not synchronous pattern of firing of the 2 O-cells. $I_{app,I} = 0.52$. Values of the other parameters are as in *C*.

is already in the theta range (without feedback), the input from the I-cells already synchronizes the O-cells, as shown above (Fig. 2). With feedback, that situation applies for some higher natural frequencies of the I-cells because the O → I coupling slows downs the I-cells. This is shown in Fig. 3*C* for natural frequency of the I-cell at 13 Hz that was slowed down to 9 Hz by the inhibitory feedback from the O-cells.

At the higher natural frequencies of the I-cell, the central effect of the feedback is to cluster the I-cell spikes into theta frequencies. This is shown in Fig. 3*D*. As the natural frequency of the I-cell increases, the number of I-cell spikes per theta cycle increases (data not shown). Thus the local I-cell frequency can be in the high gamma range while still showing theta-frequency modulation that makes it effective in synchronizing O-cells.

Heterogeneity in connections and I_h *creates a ragged theta rhythm*

In Fig. 4*A* (data from Gillies et al. 2002), we see overlaid traces from nine consecutive theta periods (~8 Hz) aligned with the peak upward deflection in concurrently recorded stratum pyramidale field potentials. The *top trace* of Fig. 4*A* corresponds to the stratum pyramidale interneurons (I), the *middle trace* corresponds to the stratum oriens (O) interneurons, and the *bottom trace* corresponds to the stratum pyramidale field. O-cells generate single action potentials (APs) on

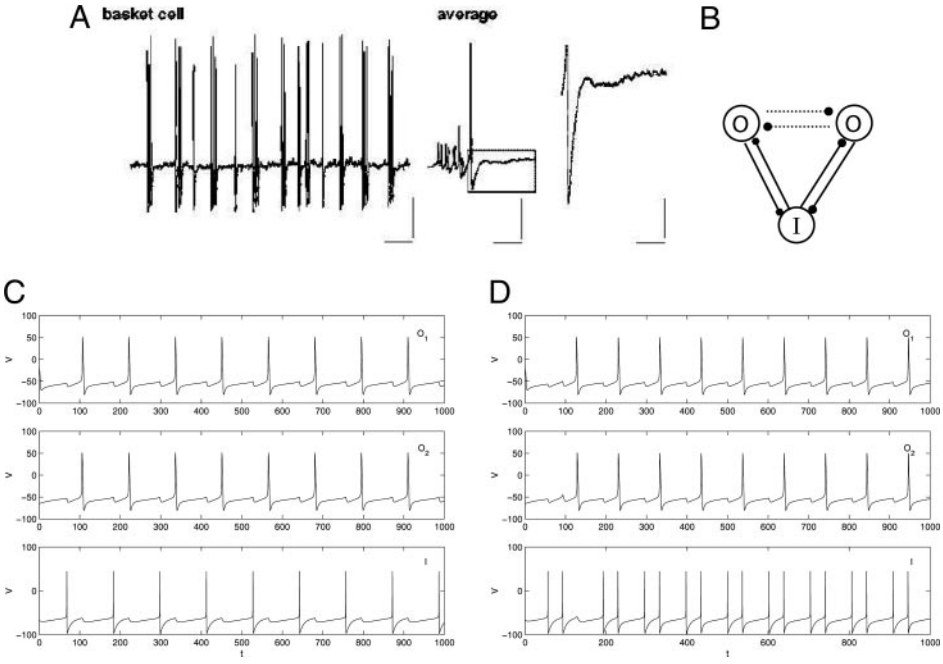

FIG. 3. Adding O–I inhibition makes network synchronize robustly at theta frequency. *A*: pattern of FS cell firing during theta oscillations in hippocampal slice; 1 to 4 action potentials are generated in bursts at theta frequencies. Burst termination is associated with a small IPSP revealed in *averaged traces* ($n = 10$ periods averaged with respect to the last spike in each burst). Scale bars: spike train 10 mV, 100 ms; average 10 mV, 25 ms; expanded average 2 mV, 10 ms. *B*: network with mutual inhibition between I- and O-cells. *C*: I-cell firing with natural frequency of about 13 Hz synchronizes the 2 O-cells and creates a coherent pattern in the presence of O → I synaptic coupling. Coupled to the network, the I-cell has a frequency of about 9.5 Hz. Values of the parameters are $G_h = 1.45$, $I_{app,O} = -1.8$, $Goo_{1,2} = Goo_{2,1} = 0.01$, $Gio_{1,2} = Gio_{2,1} = 0.2$ (as in Fig. 2); $I_{app,I} = 0.4$, $Goi_{1,2} = Goi_{2,1} = 0.08$. *D*: I-cell firing with natural frequency of about 28 Hz synchronizes the 2 O-cells in the presence of O → I synaptic coupling. $I_{app,I} = 0.52$. Values of the other parameters and initial conditions are as in *C*.

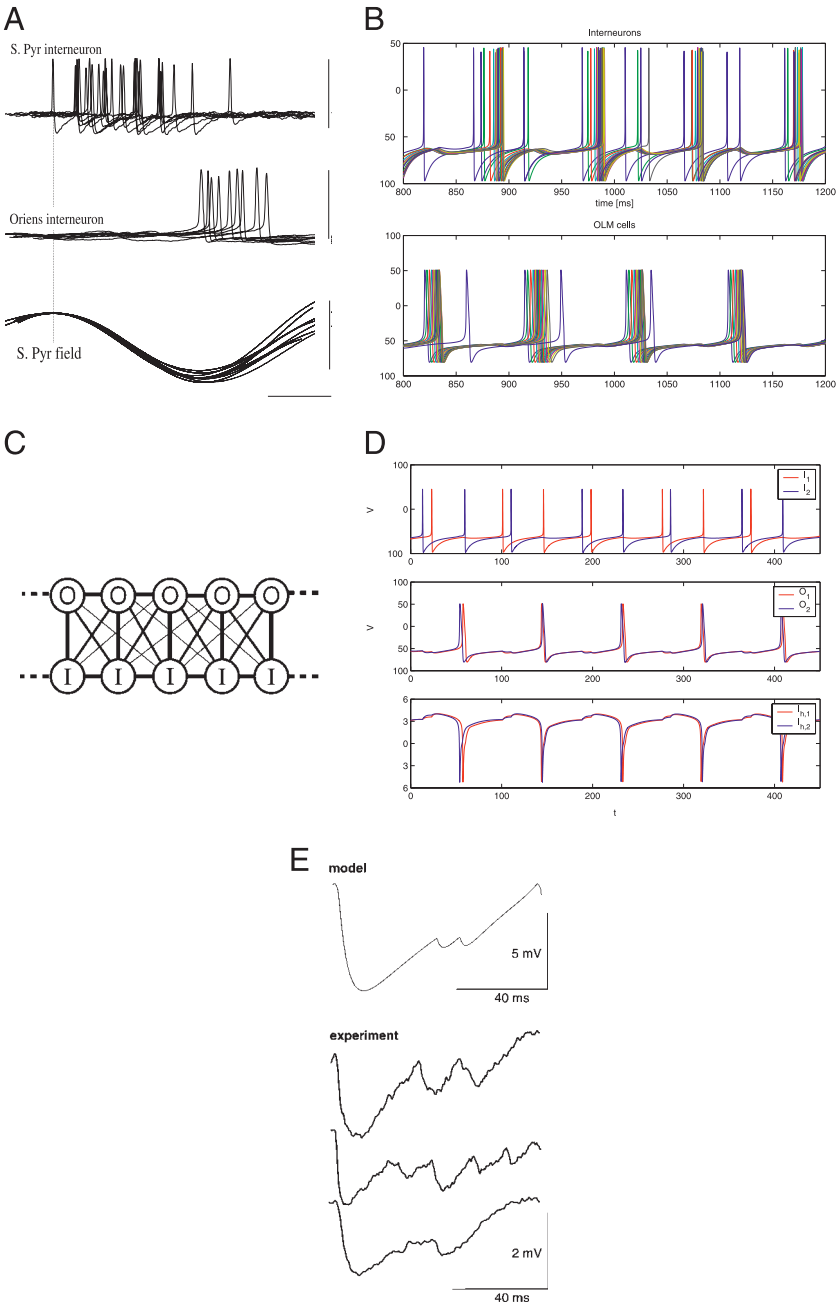

FIG. 4. If connections among O- and I-cells are made less uniform in size, "ragged synchronization" occurs similar to that seen in vitro. *A*: pattern of I-cell and O-cell spiking during field theta rhythms in area CA1 generated by DHPG in the presence of NBQX. Data shown are *9 overlaid traces* from each cell type aligned to the peak concurrently recorded field positivity. Scale bars: 20 ms, 60 mV (*intracellular spiking traces,* 0.4-mV field recording). Data reproduced from Gillies et al. (2002). *B*: schematic diagram of larger network used in Fig. 2*C*. Network has all-to-all connections with heterogeneous maximal synaptic conductivity: the closer the cells in the network, the stronger the synaptic connection. This heterogeneity is schematically represented by the thickness of the connection. For O–O and I–I we show only the strongest connections. *C*: ragged synchronization of 15 O- and 15 I-cells. Values of the parameters are $G_h = 1.45$, $I_{app,O} = -1.8$, $I_{app,I} = 0.48$, $A_{OO} = 0.01$, $A_{OI} = 0.1$, $A_{IO} = 0.072$, $A_{II} = 0.04$, $\gamma_{OO} = \gamma_{OI} = 0.002 = \gamma_{II} = 0.002$, and $\gamma_{IO} = 0.001$. *D*: ragged synchronization of 2 O- and 2 I-cells. Values of the parameters are $G_h = 1.45$, $I_{app,O} = -1.8$, $I_{app,I} = 0.41$, $Goo_{1,2} = Goo_{2,1} = 0.01$, $Gio_{1,1} = Gio_{2,2} = 0.1$; $Gio_{1,2} = Gio_{2,1} = 0.05$, $Gii_{1,1} = Gii_{2,2} = 0.04$, $Gii_{1,2} = Gii_{2,1} = 0.002$, $Goi_{1,1} = Goi_{2,2} = 0.035$, $Goi_{1,2} = Goi_{2,1} = 0.001$. *E*: pattern of model E-cell membrane potential over one period of theta oscillation revealed an initial, relatively large IPSP. Superimposed on the late decay phase of this IPSP were additional, smaller IPSPs. Scale bars: 5 mV, 40 ms. A similar pattern of pyramidal cell somatic membrane potential change was seen in each period of the theta cycle in experiment. *Three example traces* are shown to illustrate the commencement of each cycle with a large IPSP. As with the model the late decay phase of its IPSP had additional smaller IPSPs superimposed on it. In experiment the number of smaller IPSPs ranged from 5 to 1. Scale bars: 2 mV, 40 ms.

the initial rising phase of the field theta oscillations, whereas I-cells generate bursts of action potentials during the descending phase of the field theta oscillation. The superimposed traces show a consistent pattern of activity that was obtained for different O- and I-cells in several experiments: At the beginning of each theta cycle I-cells fire a large number of APs. This number decreases as the cycle is advanced and I-cells are almost silent when O-cells start firing. After the O-cells stop firing there is an interval before I-cells start firing again.

In Fig. 4*C* we show a schematic large network (see METHODS for description and parameters) of I- and O-cells. Unlike the small networks described above, each O-cell is not connected with the same strength to each I-cell and vice versa, so cells receive different amounts of inhibition. A simulation of that network (Fig. 4*B*) reproduces all the main features of the data in Fig. 4*A:* I- and O-cells fire in consecutive and slightly overlapped subintervals of the theta cycle and there is a silent subinterval of the theta cycle between the firing of O- and I-cells. Most AP activity in the I-cells is observed at the beginning of the theta cycle, and then the activity of I-cells decreases while the O-cells become active. We observed (not clearly seen in Fig. 4*B*) that each O-cell fires once per period whereas I-cells fire multiple APs. An important observation in Fig. 4*B* is that, as experimentally observed, each cell does not necessarily fire at the same phase relative to the theta cycle.

This result does not depend on the size of the network, and in fact can be reproduced in a network of two O-cells and two I-cells (Fig. 4*D*). Note that neither the I-cells nor the O-cells are completely synchronous. Furthermore, as in the data and the above simulation, the spiking of the I-cells overlaps that of the O-cells. The O-cells fire when the I_h current has built up enough by the I-cell input to spike, turning off the I-cells. The

latter, without this current, must wait until the slower-decaying O-cell inhibition wears off. The overlap occurs because the O-cells do not have to wait until the I-cell firing ceases. The same arguments apply to the larger network.

Direct comparison of theta field potential oscillations in the present model was not possible. However, field potentials can be thought of as representative of the average sum of all synaptic inputs and intrinsic membrane potential changes in a local population of principal cells (E) around the recording electrode. To compare the E-cell somatic membrane potential of the experimental situation to our model, we added an E-cell, modeled in the same way as an I-cell; the E-cell received inhibition from the O- and I-cells. In Fig. 4*E* we show that, in both model and experiment, individual theta periods began with a large IPSP. Superimposed on the late decay phase of this IPSP were additional smaller IPSPs.

DISCUSSION

The goal of this paper is to illuminate the mechanistic basis for the generation of one version of a coherent theta rhythm. The first central result is that O-cells and γ-aminobutyric acid-A ($GABA_A$)–mediated inhibition, with or without electrical coupling, cannot account for the experimentally observed coherence and dynamics. This result depends strongly on the slow, hyperpolarization-activated mixed cation current I_h, known to be expressed in O-cells (Gillies et al. 2002; Saraga et al. 2003). The second central result is that fast-spiking perisomatic targeting (FS) interneurons, known to participate in ragged synchronization (Gillies et al. 2002), can robustly entrain and synchronize O-cells, but only if the I-cells are firing at rates in the theta (8–12 Hz) range. This result depends on the fact that O-cells generate so-called rebound spikes after recovering from inhibition. O-cells are synchronized by the rebound phenomenon, which depends critically on I_h. O-cells are not entrained, and not necessarily synchronized by fast (>12 Hz) spike trains from I-cells. Our third central result is that feedback from O-cells to I-cells can regulate activity of I-cells to lie within the appropriate frequency range, allowing the network as a whole to generate coherent theta oscillations. Under the realistic assumption that connections within the network are not perfectly symmetric, this network of O- and I-cells generates "ragged synchronization" with phase relationships very similar to those seen in vitro. The network rhythm does not depend on network size and can be explained mechanistically in terms of the interactions of fast inhibition from I-cells, slow inhibition from O-cells, and the prominence of I_h in O-cells but not in I-cells.

Mechanism of coherent theta in in vitro CA1 preparation

Individual O-LM cells (O-cells) can produce a theta rhythm, but populations of them are not coherent at that frequency range. Indeed, the slow hyperpolarization-activated cation current I_h, which gives these cells their theta-rhythmic quality, is itself responsible for the lack of synchronization by mutual inhibition (see also Acker et al. 2003): when a cell expresses I_h, inhibition to that cell soon after it spikes leads to advances of the next spike, whereas later inhibition retards the next spike. The result is that, if two cells start firing close to one another, the dynamics pushes the spike times further apart (Acker et al. 2003).

Addition of FS interneurons (I-cells) to the network produces coherence in the theta-frequency range, even though the I-cells themselves are capable of firing at higher frequencies, and in fact fire at average rates well above 12 Hz even during theta synchronization. Our simulations imply that two properties of O-cells are crucial for generating a coherent theta rhythm. First, they express I_h. This current allows them to generate "rebound" spikes after inhibition. The timing of the rebound spikes, in turn, leads to increased synchronization among O-cells receiving common input. Second, O-cells are believed to give rise to slow GABAergic IPSPs postsynaptically (Gillies et al. 2002). These slow IPSPs make it easier for slowly rhythmic O-cells to impose a firing pattern on I-cells that includes significant pauses once per theta cycle. This firing pattern in I-cells is sufficient to induce the O-cells to spike synchronously by the h-current buildup mechanism described earlier. The pattern is precise for networks in which all O-cells receive identical projections from the I-cells, but realistically "ragged" when the projections from I-cells to O-cells are not uniform. The phenomenon is independent of network size.

One detail of both the experimental dynamics and the model provides an important clue to the role of I_h in the coherence mechanism: there is an overlap between the firing of the I-cells and the onset of firing of the O-cells. This overlap comes about because the I-cells not only suppress firing during some intervals, but they also prime the O-cells to generate subsequent rebound spikes. Thus, the first set of I-cell spikes can activate the O-cells and allow them to fire even while inhibition continues to arrive from the I-cells.

The model offered in this paper was able to reproduce subtle relative timing of the O-LM cells and I-cells, as well as IPSP traces in E-cells (Fig. 4). The E-cell somatic membrane potential changes were remarkably similar in model and experiment. The only discrepancy was that, in the model, two additional small IPSPs were always seen, whereas in experiment the number of smaller IPSPs was variable, ranging from five to one. This could be explained by the relatively small size of the model network compared with the available network architecture in the in vitro slice preparation. By using small networks, we were able to explain the origin of the theta coherence by the properties of I_h and the two types of inhibition in the network.

Related literature

This paper deals only with interneuronal networks that produce a theta-frequency rhythm. There is also a substantial literature, both experimental and theoretical, dealing with gamma-frequency interneuronal networks (Bragin et al. 1995; Buzsáki and Chrobak 1995; Chow et al. 1998; Gerstner et al. 1996; Jefferys et al. 1996; Lytton et al. 1996; Skinner et al. 1994; Tiesinga and Sejnowski 2004; Traub et al. 1996; van Vreeswijk et al. 1994; Wang and Buzsáki 1996; White et al. 1998, 2000a). The gamma-frequency networks have different properties because of the absence of the h-current in the model cells; this current is important for the expression of a theta rhythm (Dickson et al. 2000). The present paper extends the synchronization theory to cells that contain this ubiquitous current and to networks that contain such cells.

The model that we used for the O-cell is inspired by models of the stellate cells of the entorhinal cortex (Acker et al. 2003; Dickson et al. 2000a). For the stellate cells, the ability to

produce subthreshold and spiking theta rhythms has been traced to a persistent Na current ($I_{Na,p}$), plus I_h and/or a slow outward K-current. In this paper, we did not use the extra K-current. The I_p current we use has dynamics similar to $I_{Na,p}$, but that is not essential; it can be replaced by other currents that are slow and inward, even a tonic excitatory current. In keeping with our aim of understanding network dynamics using the simplest biophysically realistic model, our single compartment model of O-cells is less complex than the multicompartment model used by Saraga et al. (2003) to simulate back-propagating action potentials in O-cells. We believe that the differences between these two models are not important for the major conclusions of this paper.

Modeling of stellate cells is consistent with the results for this model. It was shown (Acker et al. 2003) that models of such cells synchronize with excitation, but not with fast inhibition. As we show here, they do not synchronize with slow inhibition either. The novelty of the current work is in how the two kinds of inhibition work together to create a coherent rhythm.

A more complex model that includes the O-cells is in Kunec et al. (2005). That paper investigated a model with fast-spiking interneurons, O-cells, and pyramidal cells, with external input from the medial septum, the dentate, and the entorhinal cortex. The O-cells were shown to play an important role in separating the theta rhythm into an epoch in which inputs could lead to potentiation of synapses and an epoch in which the potentiated synapses could lead to firing of unstimulated neurons.

Further modeling issues

The current model does not explicitly include NMDA currents, even though Gillies et al. (2002) reported that block of NMDA receptors affects the in vitro theta rhythm. We hypothesize that this effect of the NMDA receptor blockers is related to a feature of the NMDA receptors separate from their role in excitatory transmission: they play a role in reversing agonist-induced desensitization of mGluR5 (Alagarsamy et al. 1999b,a). Hippocampal neurons are sensitive to mGluR-dependent drive (Wang and Buzsáki 1996), and interactions between these and NMDA receptors have been reported (Awad et al. 2000; Luthi et al. 1994). In the current model, we keep the drive from mGluR receptors constant, implicitly using the NMDA effect of blocking desensitization. We do not use the kinetics of the NMDA currents; indeed, we do not use any excitatory PSPs. This is consistent with the Gillies et al. (2002) findings, in which the pyramidal cells fire exceedingly sparsely. Our model requires this sparseness because excitation from the NMDA receptors would otherwise deactivate the h-current of the O-cells necessary for the timing effects we have described.

The observation of rhythmic periods of quiescence in I-cells in experimental theta oscillations can be explained in the model entirely by input from O-cells. However, given that no direct quantification of O-cell input kinetics to I-cells is available we cannot rule out involvement of additional factors in the slice preparation or in vivo. We have used the kinetics associated with the O-cell inputs onto pyramidal cells; as shown in Fig. 4*E,* the model output is consistent with experimental data. We have more briefly investigated the effects of faster-decaying IPSPs from the O-cells. For O–O connections we found that IPSPs decaying at faster rates (down to 10 ms) create more robust antiphase solutions. We also considered O–O and O–I connections with much larger decay times (up to 40 ms) and found the results are robust with minor changes in other parameters.

In vitro experiments in CA3 suggest that a somewhat different mechanism produces a theta rhythm in that region (Gillies et al. 2002). In CA1, large enough depolarization of the slice, without blockage of AMPA-mediated excitation, produced gamma rhythms, with a suppression of the theta rhythm. This can be reproduced from our current model (Rotstein et al. 2003): when there are gamma oscillations, the I-cells fire at a gamma frequency, which, in our model, suppresses the O-cells (Netoff et al. 2004). In CA3, however, theta-frequency oscillations were more prominent (compared to CA1) in the absence of AMPA receptor blockade, with a nested gamma/theta rhythm as in Bragin et al. (1995) and Leung (1998). When AMPA receptors were blocked (Gillies et al. 2002), both gamma and theta were attenuated. Although this was not the focus of the current paper, we are also able to reproduce that result in our model by modification of the tonic drive to the O- and I-cells: the simulations modeling the CA3 data have parameters tuned so that the O- and I-cells do not fire without phasic excitation. With AMPA-mediated excitation, there is a theta rhythm nested with gamma (data not shown) (Rotstein et al. 2002).

Our simulations were designed to explain population activity observed in vitro, but it is important to note that atropine-resistant theta in slices is similar to its counterpart from in vivo recordings of neurons in urethaneanesthesized rats in CA1 (Klausberger et al. 2003). In both cases, FS interneurons fired preferentially (often more than one spike) on the descending phase of the extracellular theta oscillations recorded in the stratum pyramidale, and O-cells fired rhythmically at the trough of the theta cycles. The similarities between the data derived from our mathematical model and experimental data suggest that the interplay between I_h and synaptic interactions between heterogeneous interneuron populations may constitute an important mechanism involved in population dynamics intrinsic to the hippocampus.

APPENDIX

The inhibitory network studied in this manuscript consists of N_O O-LM (O) cells and N_I FS (I) cells. In what follows $k = 1, \ldots, N_O$ and $j = 1, \ldots, N_I$. The current-balance equations for the O- and I-cells are

$$C_O \, \mathrm{d}v_{O,k}/\mathrm{d}t = I_{app,O} - I^k_{O,Na} - I^k_{O,K} - I^k_{O,L} - I^k_{O,p} - I^k_h - I\,syn_{O,k}$$

and

$$C_I \, \mathrm{d}v_{I,j}/\mathrm{d}t = I_{app,I} - I^j_{I,Na} - I^j_{I,K} - I^j_{I,L} - I\,syn_{I,j}$$

respectively, where $v_{\mathrm{O,k}}$ and $v_{\mathrm{I,j}}$ are the membrane potentials (mV), C_O and C_I are the membrane capacitances (μF/cm^2), $I_{app,O}$ and $I_{app,I}$ are the applied bias (DC) current (μA), and the ionic and synaptic currents are given by

$$I^k_{O,Na} = G_{O,Na}\, m^3_{O,k}\, h_{O,k}(v_{O,k} - E_{O,Na})$$

$$I^k_{O,K} = G_{O,K}\, n^4_{O,k}(v_{O,k} - E_{O,K})$$

$$I^k_{O,L} = G_{O,L}(v_{O,k} - E_{O,L})$$

$$I^k_{O,p} = G_p\, p_{O,k}(v_{O,k} - E_{O,Na})$$

$$I^k_{O,h} = G_h(0.65h^f_{O,k} + 0.35h^s_{O,k})(v_{O,k} - E_h)$$

$$I^j_{I,Na} = G_{I,Na}\, m^3_{I,j}\, h_{I,j}(v_{I,j} - E_{I,Na})$$

$$I^j_{I,K} = G_{I,j}\, n^4_{I,j}(v_{I,j} - E_{I,j})$$

$$I^j_{I,L} = G_{I,L}(v_{I,j} - E_{I,L})$$

$$I\ syn_{O,k} = \sum_{i=1,i\neq k}^{N_O} G_{OO,i,k}\, S_{OO,i}(v_{O,k} - E_{in}) + \sum_{i=1}^{N_I} G_{IO,i,k}\, S_{IO,i}(v_{O,k} - E_{in})$$

and

$$I\ syn_{I,j} = \sum_{i=1}^{N_O} G_{OI,i,j}\, S_{OI,i}(v_{I,j} - E_{in}) + \sum_{i=1}^{N_I} G_{II,i,j}\, S_{II,i}(v_{I,j} - E_{in})$$

In the expressions for the different currents I_X, G_X are the maximal conductances (mS/cm^2) and E_X are the reversal potentials (mV). Units of time are ms. All the dynamics variables $x_{O,k} = m_{O,k}$, $h_{O,k}$, $n_{O,k}$, $p_{O,k}$, $h^f_{O,k}$, and $h^s_{O,k}$ obey a first-order differential equation of the following form

$$\mathrm{d}x_{O,k}/\mathrm{d}t = [x_{O,\infty}(v_{O,k}) - x_{O,k}]/\tau_{x_O}(v_{O,k})$$

where

$$x_{O,\infty}(v_{O,k}) = \alpha_{x_O}(v_{O,k})/[\alpha_{x_O}(v_{O,k}) + \beta_{x_O}(v_{O,k})]$$

$$\tau_{x_O}(v_{O,k}) = 1/[\alpha_{x_O}(v_{O,k}) + \beta_{x_O}(v_{O,k})]$$

and

$$\alpha_{m_O}(v) = -0.1(v + 23)/[e^{-0.1(v+23)} - 1]$$

$$\beta_{m_O}(v) = 4e^{-(v+48)/18}$$

$$\alpha_{h_O}(v) = 0.07e^{-(v+37)/20}$$

$$\beta_{h_O}(v) = 1/[e^{-0.1(v+7)} + 1]$$

$$\alpha_{n_O}(v) = -0.01(v + 27)/[e^{-0.1(v+27)} - 1]$$

$$\beta_{n_O}(v) = 0.125e^{-(v+37)/80}$$

$$\alpha_{p_O}(v) = 1/\{0.15[1 + e^{-(v+38)/6.5}]\}$$

$$\beta_{p_O}(v) = e^{-(v+38)/6.5}/\{0.15[1 + e^{-(v+38)/6.5}]\}$$

$$h^f_{O,\infty}(v_{O,k}) = 1/[1 + e^{(v+79.2)/9.78}]$$

$$\tau_{h^f_O}(v_{O,k}) = 0.51/[e^{(v-1.7)/10} + e^{-(v+340)/52}] + 1$$

$$h^s_{O,\infty}(v_{O,k}) = 1/[1 + e^{(v+2.83)/15.9}]^{58}$$

$$\tau_{h^s_O}(v_{O,k}) = 5.6/[e^{(v-1.7)/14} + e^{-(v+260)/43}] + 1$$

All the dynamic variables $x_{I,k} = m_{I,k}$, $h_{I,k}$, $n_{I,k}$ obey a first-order differential equation of the following form

$$\mathrm{d}x_{I,k}/\mathrm{d}t = [x_{I,\infty}(v_{I,k}) - x_{I,k}]/\tau_{x_I}(v_{I,k})$$

where

$$x_{I,\infty}(v_{I,k}) = \alpha_{x_I}(v_{I,k})/[\alpha_{x_I}(v_{I,k}) + \beta_{x_I}(v_{I,k})]$$

$$\tau_{x_I}(v_{I,k}) = 1/[\alpha_{x_I}(v_{I,k}) + \beta_{x_I}(v_{I,k})]$$

and

$$\alpha_{m,I}(v) = 0.32(54 + v)/[1 - e^{-(v+54)/4}]$$

$$\beta_{m,I}(v) = 0.28(v + 27)/[e^{(v+27)/5} - 1]$$

$$\alpha_{h,I}(v) = 0.128e^{-(50+v)/18}$$

$$\beta_{h,I}(v) = 4/[1 + e^{-(v+27)/5}]$$

$$\alpha_{n,I}(v) = 0.032(v + 52)/[1 - e^{-(v+52)/5}]$$

$$\beta_{n,I}(v) = 0.5e^{-(57+v)/40}$$

The synaptic variables S_{XZ} ($X, Z = O, I$) obey first-order differential equations of the form

$$\mathrm{d}S_{XZ,k}/\mathrm{d}t = NT_{XZ}(v_{X,k})(1 - S_{XZ,k}) - \beta_{XZ}S_{XZ,k}$$

where

$$NT_{XZ}(v) = \frac{\alpha_{XZ}}{2}\{1 + \tanh[(v - Vth_{XZ})/Vsl_{XZ}]\}$$

The values of the parameters used in our simulations are $E_{O,Na} = 55$, $E_{O,K} = -90$, $E_h = -20$, $E_{O,L} = -65$, $G_{O,Na} = 52$, $G_{O,K} = 11$, $G_{O,L} = 0.5$, $G_{O,p} = 0.5$, $C_O = 1$, $E_{I,Na} = 50$, $E_{I,K} = -100$, $E_{I,L} = -67$, $G_{I,Na} = 100$, $G_{I,K} = 80$, $G_{I,L} = 0.1$, $G_h = 1.46$, $I_{app,O} = -1.8$, $I_{app,I} = 0.48$, $E_{in} = -80$, $\alpha_{OZ} = 5$, $\beta_{OZ} = 0.05$, when $Z = 0, I$, $\alpha_{IZ} = 15$, $\beta_{IZ} = 0.11$, when $Z = O, I, E$, $\alpha_{EZ} = 20$, $\beta_{EZ} = 0.12$, when $Z = O,I$, $Vth_{XZ} = 0$, $V\,sl_{XZ} = 0.1$, when $X, Z = O, I$.

The synaptic maximal conductances are given by

$$G_{OO,ik} = \begin{cases} A_{OO}e^{-\gamma_{OO}(i-k)^2} & 1 \le i, k \le N_O \\ 0 & \text{otherwise} \end{cases}$$

$$G_{IO,jk} = \begin{cases} A_{IO}e^{-\gamma_{IO}(i-k)^2} & 1 \le i \le N_I, 1 \le k \le N_O \\ 0 & \text{otherwise} \end{cases}$$

$$G_{OI,jk} = \begin{cases} A_{OI}e^{-\gamma_{OI}(i-j)^2} & 1 \le i \le N_O, 1 \le j \le N_I \\ 0 & \text{otherwise} \end{cases}$$

$$G_{II,jk} = \begin{cases} A_{II}e^{-\gamma_{II}(i-j)^2} & 1 \le i, j \le N_I \\ 0 & \text{otherwise} \end{cases}$$

The dynamical model of the E-cell is identical to the one for the I-cell, with the exception of the synaptic variable, which was omitted because E-cell's output is not used in this paper.

ACKNOWLEDGMENTS

We are grateful to G. Buzsáki, E. Sivan, and S. Epstein for reading earlier versions of this manuscript and for helpful comments and to G. Duffy for help preparing some of the figures.

GRANTS

This work was partially supported by the Burroughs Wellcome Fund to H. G. Rotstein and N. Kopell, National Institute of Neurological Disorders and Stroke Grants R01 NS-46058-2 as part of the Collaborative Research in Computational Neuroscience Program to M. A. Whittington, N. Kopell, and H. G. Rotstein and R01 NS-34425 to J. A. White, the Medical Research Council of the United Kingdom and Wellcome Trust to M. A. Whttington.

REFERENCES

Acker CD, Kopell N, and White JA. Synchronization of strongly coupled excitatory neurons: relating network behavior to biophysics. *J Comput Neurosci* 15: 71–90, 2003.

Alagarsamy S, Marino MJ, Rouse ST, Gereau RW IV, Heinemann SF, and Conn PJ. Activation of NMDA receptors reverses desensitization of mGluR5 in native and recombinant systems. *Nat Neurosci* 2: 234–240, 1999b.

Alagarsamy S, Rouse ST, Gereau RW IV, Heinemann SF, Smith Y, and Conn PJ. Activation of *N*-methyl-D-aspartate receptors reverses desensitization of metabotropic glutamate receptor, mGluR5, in native and recombinant systems. *Ann NY Acad Sci* 868: 526–530, 1999a.

Ali A and Thomson A. Facilitating pyramid to horizontal oriensalveus interneurone inputs: dual intracellular recordings in slices of rat hippocampus. *J Physiol* 507: 185–199, 1998.

Alonso AA and Llinás RR. Subthreshold Na^+-dependent theta like rhythmicity in stellate cells of entorhinal cortex layer II. *Nature* 342: 175–177, 1989.

Awad H, Hubert GW, Smith Y, Levey AI, and Conn PJ. Activation of metabotropic glutamate receptor 5 has direct excitatory effects and potentiates NMDA receptor currents in neurons of the subthalamic nucleus. *J Neurosci* 20: 7871–7879, 2000.

Banks MI, White JA, and Pearce RA. Interactions between distinct GABA(A) circuits in hippocampus. *Neuron* 25: 449–457, 2000.

Bland BH and Colom LV. Extrinsic and intrinsic properties underlying oscillation and synchrony in limbic cortex. *Prog Neurobiol* 41: 157–208, 1993.

Bragan A, Jando G, Nadasdy Z, Hetke J, Wise K, and Buzsáki G. Gamma (40–100 Hz) oscillation in the hippocampus of the behaving rat. *J Neurosci* 15: 47–60, 1995.

Burden RL and Faires JD. *Numerical Analysis.* Boston, MA: PWS, 1980.

Buzsáki G. Two-stage model of memory trace formation: a role for "noisy" brain states. *Neuroscience* 31: 551–570, 1989.

Buzsáki G. Theta oscillations in the hippocampus. *Neuron* 33: 325–340, 2002.

Buzsáki G and Chrobak JJ. Temporal structure in spatially organized neuronal ensembles: a role for interneuronal networks. *Curr Opin Neurobiol* 5: 504–510, 1995.

Buzsáki G, Czopf J, Kondakor I, and Kellenyi L. Laminar distribution of hippocampal rhythmic slow activity (RSA) in the behaving rat: current source density analysis, effects of urethane and atropine. *Brain Res* 365: 125–137, 1986.

Buzsáki G, Leung LW, and Vanderwolf CH. Cellular bases of hippocampal EEG in the behaving rat. *Brain Res* 287: 139–171, 1983.

Chapman CA and Lacaille JC. Cholinergic induction of theta-frequency oscillations in hippocampal inhibitory interneurons and pacing of pyramidal cell firing. *J Neurosci* 19: 8637–8645, 1999a.

Chapman CA and Lacaille JC. Intrinsic theta-frequency membrane potential oscillations in hippocampal CA1 interneurons of stratum lacunosum-moleculare. *J Neurophysiol* 81: 1296–1307, 1999b.

Chow CC, White JA, Ritt J, and Kopell N. Frequency control in synchronous networks of inhibitory neurons. *J Comput Neurosci* 5: 407–420, 1998.

Crook SM, Ermentrout GB, and Bower JM. Spike frequency adaptation affects the synchronization properties of networks of cortical oscillations. *Neural Comput* 10: 837–854, 1998.

Csicsvari J, Jamieson B, Wise KD, and Buzsáki G. Mechanisms of gamma oscillations in the hippocampus of the behaving rat. *Neuron* 37: 311–322, 2003.

Dickson CT, Magistretti J, Shalinsky MH, Fransén E, Hasselmo M, and Alonso AA. Properties and role of I_h in the pacing of subthreshold oscillation in entorhinal cortex layer II neurons. *J Neurophysiol* 83: 2562–2579, 2000.

Ermentrout B. *Simulating, Analyzing, and Animating Dynamical Systems. A Guide to XPPAUT for Researchers and Students.* Philadelphia, PA: Soc. for Industr. & Appl. Math., 2002.

Fellous JM and Sejnowski TJ. Cholinergic induction of oscillations in the hippocampal slice in the slow (0.5–2 Hz), theta (5–12 Hz), and gamma (25–70 Hz) bands. *Hippocampus* 10: 187–197, 2000.

Fox SE, Wolfson S, and Ranck JBJ. Hippocampal theta rhythm and the firing of neurons in walking and urethane anesthetized rats. *Exp Brain Res* 62: 495–508, 1986.

Gerstner W, van Hemmen JL, and Cowen J. What matters in neuronal locking? *Neural Comput* 8: 1653–1676, 1996.

Gillies MJ, Traub RD, LeBeau FEN, Davies CH, Gloveli T, Buhl EH, and Whittington MA. A model of atropine-resistant theta oscillations in rat hippocampal area CA1. *J Physiol* 543.3: 779–793, 2002.

Hájos N and Mody I. Synaptic communication among hippocampal interneurons: properties of spontaneous IPSCs in morphologically identified cells. *J Neurosci* 17: 8427–8442, 1997.

Harris KD, Henze DA, Csicsvari J, Hirase H, and Buzsáki G. Accuracy of tetrode spike separation as determined by simultaneous intracellular and extracellular measurements. *J Neurophysiol* 84: 401–414, 2000.

Hoppensteadt FC and Izhikevitch EM. *Weakly Connected Neural Networks.* New York: Springer-Verlag, 1997.

Jefferys J, Traub R, and Whittington M. Neuronal networks for induced "40 Hz" rhythms. *Trends Neurosci* 19: 202–208, 1996.

Jouvet M. Biogenic amines and the states of sleep. *Science* 163: 32–41, 1969.

Kahana MJ, Sekuler R, Caplan JB, Kirschen M, and Madsen JR. Human theta oscillations exhibit task dependence during virtual maze navigation. *Nature* 399: 781–784, 1999.

Kamondi A, Acsady L, Wang XJ, and Buzsáki G. Theta oscillations in somata and dendrites of hippocampal pyramidal cells in vivo: activity-dependent phase-precession of action potentials. *Hippocampus* 8: 244–261, 1998.

Klausberger T, Magill PJ, Márton LF, Roberts JDB, Cobden PM, Buzsáki G, and Somogyi P. Brain-state- and cell-type-specific firing of hippocampal interneurons *in vivo. Nature* 421: 844–848, 2003.

Kocsis B, Bragin A, and Buzsáki G. Interdependence of multiple theta generators in the hippocampus: a partial coherence analysis. *J Neurosci* 19: 6200–6212, 1999.

Konopacki J, Bland BH, MacIver MB, and Roth SH. Cholinergic theta rhythm in transected hippocampal slices: independent CA1 and dentate generators. *Brain Res* 436: 217–222, 1987.

Kopell N and LeMasson G. Rhythmogenesis, amplitude modulation, and multiplexing in a cortical architecture. *Proc Natl Acad Sci USA* 91: 10586–10590, 1994.

Kunec S, Hasselmo M, and Kopell N. Encoding and retrieval in the CA3 region of the hippocampus: a model of theta phase separation. *J Neurophysiol* 94: 70–82, 2005.

Lacaille J-C, Williams S, Kunkel D, and Schwartzkroin P. Local circuit interactions between oriens/alveus interneurons and CA1 pyramidal cells in hippocampal slices: electrophysiology and morphology. *J Neurosci* 7: 1979–1993, 1987.

Larson J and Lynch G. Induction of synaptic potentiation in hippocampus by patterned stimulation involves two events. *Science* 232: 985–988, 1986.

Lee MG, Chrobak JJ, Sik A, Wiley RG, and Buzsáki G. Hippocampal theta activity following selective lesion of the septal cholinergic system. *Neuroscience* 62: 1033–1047, 1994.

Leung LS. Generation of theta and gamma rhythms in the hippocampus. *Neurosci Biobehav Rev* 22: 275–290, 1998.

Lisman JE and Idiart JA. Storage of 7 ± 2 short term memories in oscillatory subcycles. *Science* 267: 1512–1515, 1995.

LoFaro T and Kopell N. Timing regulation in a network reduced from voltage-gated equations to a one-dimensional map. *J Math Biol* 38: 479–533, 1999.

Luthi A, Gahwiler BH, and Gerber U. Potentiation of a metabotropic glutamatergic response following NMDA receptor activation in rat hippocampus. *Pflügers Arch* 427: 197–202, 1994.

Lytton WW. Optimizing synaptic conductance calculation for network simulations. *Neural Comput* 8: 501–509, 1996.

Lytton WW, Destexhe A, and Sejnowski TJ. Control of slow oscillations in the thalamocortical neuron: a computer model. *Neuroscience* 70: 674–684, 1996.

Maccaferri G and McBain C. The hyperpolarization-activated current (I_h) and its contribution to pacemaker activity in rat CA1 hippocampal stratum oriens-alveus interneurones. *J Physiol* 497: 119–130, 1996.

Nadim F, Manor Y, Kopell N, and Marder E. Synaptic depression creates a switch that controls the frequency of an oscillator circuit. *Proc Natl Acad Sci USA* 96: 8206–8211, 1999.

Netoff TI, Pervouchine D, Kopell N, and White JA. Oscillation frequency switches in model and hybrid networks of the hippocampus. *Soc Neurosci Abstr* 741.4, 2004.

O'Keefe J. Hippocampus, theta, and spatial memory. *Curr Opin Neurobiol* 3: 917–924, 1993.

O'Keefe J and Nadel L. *The Hippocampus as a Cognitive Map.* Oxford, UK: Clarendon, 1978.

O'Keefe J and Recce ML. Phase relationship between hippocampal place units and the EEG theta rhythm. *Hippocampus* 3: 317–330, 1993.

Raghavachari S, Kahana JJ, Rizzuto DS, Caplan JB, Kirschen MP, Bourgeois M, Madsen JR, and Lisman JE. Gating of human theta oscillations by a working memory task. *J Neurosci* 21: 3175–3183, 2001.

Rotstein HG, Gillies MJ, Acker CD, White JA, Whittington MA, and Kopell N. Slow and fast inhibition and h-current interact to create a theta rhythm in CA1. *Soc Neurosci Abstr* 258.3, 2003.

Rotstein HG, Gillies MJ, Whittington MA, Buhl EH, and Kopell N. A model of an inhibition-based atropine-resistant theta frequency oscillation in CA1 in vitro. *Soc Neurosci Abstr* 753.10, 2002.

Saraga F, Wu CP, Zhang L, and Skinner FK. Active dendrites and spike propagation in multi-compartment models of oriens-lacunosum/moleculare hippocampal interneurons. *J Physiol* 552.3: 502–509, 2003.

Skaggs WE, McNaughton BL, Wilson MA, and Barnes CA. Theta phase precession in hippocampal neuronal populations and the compression of temporal sequences. *Hippocampus* 6: 149–172, 1996.

Skinner FK, Kopell N, and Marder E. Mechanisms for oscillations and frequency control in networks of mutually inhibitory relaxation oscillators. *J Comput Neurosci* 1: 69–87, 1994.

Squire LR and Zola-Morgan S. The medial temporal lobe memory system. *Science* 253: 1380–1386, 1991.

Stewart M and Fox SE. Do septal neurons pace the hippocampal theta rhythm? *Trends Neurosci* 13: 163–168, 1990.

Tiesinga PH and Sejnowski TJ. Rapid temporal modulation of synchrony by competition in cortical interneuron networks. *Neural Comput* 16: 251–275, 2004.

Traub RD, Whittington MA, Colling SB, Buzsáki G, and Jefferys JG. Analysis of gamma rhythms in the rat hippocampus *in vitro* and *in vivo*. *J Physiol* 493: 471–484, 1996.

Vanderwolf CH. Hippocampal electrical activity and voluntary movement in the rat. *Clin Neurophysiol* 26: 407–418, 1969.

van Vreeswijk C, Abbott LF, and Ermentrout GB. When inhibition not excitation synchronizes neural firing. *J Comput Neurosci* 1: 313–322, 1994.

Wang X-J and Buzsáki G. Gamma oscillations by synaptic inhibition in an interneuronal network model. *J Neurosci* 16: 6402–6413, 1996.

Wang X-J and Rinzel J. Alternating and synchronous rhythms in reciprocally inhibitory model neurons. *Neural Comput* 4: 84–97, 1992.

White JA, Banks MI, Pearce RA, and Kopell N. Networks of interneurons with fast and slow gamma-aminobutyric acid type A (GABAA) kinetics provide substrate for mixed gamma-theta rhythm. *Proc Natl Acad Sci USA* 97: 8128–8133, 2000.

White JA, Chow CC, Ritt J, Soto-Treviño C, and Kopell N. Synchronization and oscillatory dynamics in heterogeneous, mutually inhibitory networks. *J Comput Neurosci* 5: 5–16, 1998.

Whittington MA and Traub RD. Interneuron diversity series: inhibitory interneurons and network oscillations in vitro. *Trends Neurosci* 26: 676–682, 2003.

Williams JH and Kauer JA. Properties of carbachol-induced oscillatory activity in rat hippocampus. *J Neurophysiol* 78: 2631–2640, 1997.